Journal Name

Dynamic Article Links ►

For published version please see: DOI: 10.1039/c4cp04095c

www.rsc.org/xxxxxx

ARTICLE TYPE

Probing a Chemical Compass: Novel Variants of Low-Frequency Reaction Yield Detected Magnetic Resonance.

Kiminori Maeda,[a,b,‡] Jonathan G. Storey,[a,‡] Paul A. Liddell,[c] Devens Gust,[c] P. J. Hore,[d] C. J. Wedge[e,*] and Christiane R. Timmel[a,*]

Received (in XXX, XXX) Xth XXXXXXXXX 20XX, Accepted Xth XXXXXXXXX 20XX

DOI: 10.1039/c4cp04095c

We present a study of a carotenoid-porphyrin-fullerene triad previously shown to function as a chemical compass: the photogenerated carotenoid-fullerene radical pair recombines at a rate sensitive to the orientation of an applied magnetic field. To characterize the system we develop a time-resolved Low-Frequency Reaction Yield Detected Magnetic Resonance (tr-LF-RYDMR) technique; the effect of varying the relative orientation of applied static and 36 MHz oscillating magnetic fields is shown to be strongly dependent on the strength of the oscillating magnetic field. RYDMR is a diagnostic test for involvement of the radical pair mechanism in the magnetic field sensitivity of reaction rates or yields, and has previously been applied in animal behavioural experiments to verify the involvement of radical-pair-based intermediates in the magnetic compass sense of migratory birds. The spectroscopic selection rules governing RYDMR are well understood at microwave frequencies for which the so-called 'high-field approximation' is valid, but at lower frequencies different models are required. For example, the breakdown of the rotating frame approximation has recently been investigated, but less attention has so far been given to orientation effects. Here we gain physical insights into the interplay of the different magnetic interactions affecting low-frequency RYDMR experiments performed in the challenging regime in which static and oscillating applied magnetic fields as well as internal electron-nuclear hyperfine interactions are of comparable magnitude. Our observations aid the interpretation of existing RYDMR-based animal behavioural studies and will inform future applications of the technique to verify and characterize further the biological receptors involved in avian magnetoreception.

Introduction

It was proposed over three decades ago that biological radical pairs, as described by the radical pair mechanism (RPM), may be responsible for the magnetic sense of migratory birds,[1] yet only relatively recently have quantitative studies lent weight to this hypothesis.[2, 3] The investigations include animal behavioural studies[4-6] and spectroscopic characterisation of the proposed radicals[7, 8] as well as detailed theoretical descriptions.[9-13] At the heart of this recent work is the protein cryptochrome[13, 14] whose photoinduced radical pairs have been shown to exhibit magnetic field effects (MFEs) *in vitro*[8, 15]. However, up to now only one molecule, namely a carotenoid-porphyrin-fullerene (CPF) triad model system,[16] Scheme 1, has been shown to be capable of detecting the orientation as well as the magnitude of an applied magnetic field and hence act as a compass.[17] Here we probe the magnetic properties of this molecule, which allow such an anisotropic response to occur, in experiments combining weak static and oscillating magnetic fields. These combined fields generate a response which is much more structured and informative than the broad spectrum obtained by application of a static field alone.

Low-frequency Reaction Yield Detected Magnetic Resonance (LF-RYDMR) has previously been proposed as a diagnostic test for involvement of the RPM[18, 19] and animal behavioural studies have indeed shown that oscillating magnetic fields can disrupt the magnetic sense of migratory birds, an effect strongly dependent on the angle between the geomagnetic and the oscillating fields.[5, 6] Several studies have been conducted to prove that this is a genuine resonance phenomenon (although a recent study also provides evidence against a resonant effect[20]). For example, it was shown that a 15 nT oscillating field can disrupt migratory orientation when applied at a frequency matching the (static) field-induced energy-level splittings within the radical pair. However, oscillating fields at half or double the expected resonance frequency were ineffective at disorienting the birds even when the strength of the RF field was increased by an order of magnitude.[4] If independently verified, such studies will provide strong evidence for an RPM based compass sense. However, animal experiments are limited to a small number of discrete experimental conditions and thus can only provide qualitative information; *i.e.* whether normal magnetic orientation is retained or disrupted in the presence of an oscillating magnetic field. The present study of the CPF triad system informs the

interpretation of the zoological observations, with data available across a wide range of oscillating and static field strengths. It also allows the effect of the relative orientation of the fields to be investigated in detail, a non-trivial task as the typically employed high-field models of magnetic resonance are not applicable.

It has been reported that oscillating fields applied parallel to the geomagnetic field do not cause migratory disorientation in the European Robin, yet when the two fields are oriented at an angle of 24° the animals lost their ability to use their magnetic compass.[5, 6] The high-field selection rules typically employed in magnetic resonance spectroscopy require a component of the oscillating field perpendicular to the external magnetic field for any resonant transition, but break down for the weak static fields employed in these animal studies. Here, we combine experimental investigations with detailed theoretical models and simulations to develop our understanding of the spin dynamics of the radical pairs in such weak fields. We believe that the results of our study will aid the design and interpretation of *in vivo* experiments aimed at determining the origin of the avian compass sense.[4-6]

From a thermodynamic standpoint the energy of interaction of an unpaired electron with an applied magnetic field is significantly lower than typical bond energies (and many orders of magnitude smaller than the thermal energy, k_BT). Hence, the notion that magnetic fields may affect any radical pair process may seem farfetched. However, radical pairs are often created with their spin systems far from thermal equilibrium, typically by photolysis, electron transfer or H-abstraction. Conservation of total spin angular momentum, S, from their molecular precursors results in a spin-correlated singlet ($S = 0$) or triplet state ($S = 1$). In the absence of any inter-radical interactions and external magnetic fields the singlet and all three triplet (T_0, T_+, T_-) states have similar energies and interconversion between them is driven by the magnetic interactions between electron and nuclear spins (the hyperfine couplings). The Zeeman effect of an applied magnetic fields energetically isolates T_+ and T_- from the S/T_0 manifold and decelerates singlet-triplet interconversion (see Figure 1B for a pictorial illustration in the limit of high field). Thus the yield and/or rate of any spin-selective reaction to singlet (or triplet) products may be affected directly by the magnetic fields applied.[21]

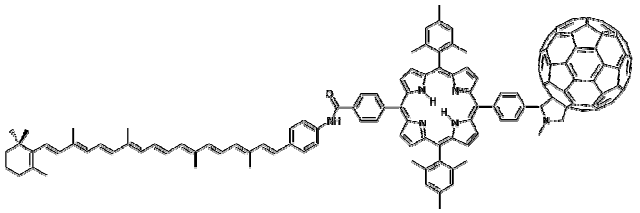

Scheme 1. Structure of the CPF triad

In conventional RYDMR experiments an oscillating field is applied in addition and oriented perpendicularly to the static field. If in resonance with energy splittings within the radical pair the oscillating field serves to boost ST mixing efficiency, altering the reaction yields and/or radical pair lifetimes. The RYDMR technique was initially developed at the microwave frequencies conventionally used in Electron Paramagnetic Resonance (EPR)[22-25] but has recently been applied using radiofrequency (RF) fields.[18, 19, 26-28] Interpretation of LF-RYDMR data is particularly challenging because the interactions of the electron spins with the applied fields and the surrounding magnetic nuclei are of comparable magnitude. As a consequence, the $T_\pm$ states are not fully isolated and various simplifying approximations applicable at high field break down: (i) transitions become at least partially allowed at virtually all orientations of the static and oscillating fields,[18, 26] and (ii) the rotating frame approximation used in high-field simulations to remove the time-dependence of the spin Hamiltonian becomes invalid.[27, 29] So far LF-RYDMR studies have been limited to continuous-wave techniques based on fluorescence detection of the reaction yield.[19, 27-29] Here we present a time-resolved transient absorption based LF-RYDMR experiment which is applicable to a much wider range of systems and provides additional information on the time-evolution of the spin system.

The chemical compass investigated here is a biradical formed photochemically from a triad consisting of carotenoid (C), porphyrin (P) and fullerene (F) moieties, Scheme 1. Green light excitation of the porphyrin generates a singlet state from which rapid and irreversible electron transfer forms the primary radical pair $^1[CP^{\bullet+}F^{\bullet-}]$, followed by a rapid electron transfer to produce $^1[C^{\bullet+}PF^{\bullet-}]$ in high yield, Figure 1A. Although the inter-spin coupling in the primary radical pair is strong, precluding any significant spin mixing, the final charge-separated state has a considerably lower electronic exchange coupling ($J = 0.17$ mT)[30] allowing efficient singlet–triplet mixing and hence the formation of a large MFE.[17] The relatively long lifetime of the radical pair state (approx. 1 μs)[17] has allowed observation of MFEs from fields as weak as that of the Earth. Moreover, experiments conducted in fixed matrices (liquid crystals and frozen glasses) proved unambiguously that the magnetoresponse of the radical pairs was strongly dependent upon the orientation of the CPF triad molecule within an applied magnetic field.[17]

Experimental

The CPF triad was synthesized according to the previously published procedure.[16] All experiments were performed using ~100 μM frozen-solutions of CPF in 2-methyltetrahydrofuran (MeTHF). The radical pair was generated from the ground state molecule using a photolysis flash of wavelength 532 nm provided by a frequency-doubled Nd:YAG laser (Continuum Surelite I operating at 10 Hz, producing 7 ns, 5 mJ pulses).

EPR experiments were performed on an X-band Bruker E680 pulsed spectrometer using a 5 mm dielectric resonator (MD5) within an Oxford helium cryostat. The laser was mounted so as to allow horizontal access through the optical window of the cavity and aligned for maximum transient EPR signal intensity using a single turning prism. Optimal microwave pulse lengths were determined from the results of nutation experiments [See ESI†]. Owing to rapid loss of phase-coherence in the pulsed EPR experiments it was not possible to observe a spin-echo. Consequently, in all experiments discussed the signal was obtained by using a π/2 pulse to generate a free induction decay (FID). Due to fast recombination from the singlet biradical state the FID decays rapidly limiting the length of the detection time window in which the FID can be observed. Along with the deadtime following the microwave pulse, this limits the spectral bandwidth and after phase correction the absolute signal phase is therefore arbitrary.

LF-RYDMR experiments employed a transient absorption technique similar to that described previously.[17] The probe beam was provided by a 975 nm 1 W diode laser (Thorlabs L975P1WJ) which was depolarised and collimated prior to passing through the sample cell. The monitoring light exiting the sample was detected by a photomultiplier tube (Hamamatsu R5108) protected from scattered light by an interference filter angled for maximum signal transmission (Comar Instruments 980IL25). Transients were collected on a digital oscilloscope (LeCroy WaveSurfer 42Xs) synchronised to the pulsed laser using a photodiode. Data throughout the paper are displayed in terms of ΔA, the difference in the absorbance of the sample in the presence and absence of the photolysis beam. The sample was mounted in a 5 mm Suprasil cuvette (3 mm optical path length) cooled using a flow of cold nitrogen gas within a quartz Dewar insert of standard design. As dictated by the optimal dielectric properties of the frozen solvent at this temperature, all experiments were performed at approximately 120 K.[31] Under these conditions some molecular tumbling may occur and observation of anisotropic MFEs is not expected. The static magnetic field (B_0) was applied using two perpendicular pairs of Helmholtz coils, capable of producing a field at any angle (θ) within the plane of the laser table, as described previously.[17] The linearly-polarized RF field (B_1) was generated using a pair of flat spiral coils (separation and outer diameter 16 mm, inner diameter 10 mm, 3 turns each side), which fitted between the static field coils and cryostat of the existing apparatus. The alignment of the RF coils was such that their field was parallel to the probe beam which in this study was defined as the $\theta = 0°$ orientation of the static field [Diagram in ESI†].

The transient absorption apparatus may be used in a number of modes to perform different experiments. (i) In the absence of oscillating fields, subtracting the transients recorded in the presence and absence of a static field allows determination of the normal static MFE (Magnetically Altered Reaction Yield, MARY) as in ref. 17. In LF-RYDMR experiments the static field is present throughout every transient, but spectra are obtained by subtraction of data recorded in the presence and absence of the RF field. (ii) For a field-swept LF-RYDMR experiment the static field strength is varied in order to build up a spectrum. During these experiments, the angle between the RF field and the static field is held constant. (iii) In the rotary-RYDMR experiment the strengths of the static and oscillating fields and the RF frequency (ν_{RF}) are held constant while the relative orientation of the applied fields is varied. For rotary-RYDMR, data are usually collected under the condition that the oscillation frequency matches the Zeeman splitting (the energy gap between the S/T_0 and the $T_{+/-}$ manifold, ~28.0 MHz/mT) in the radical pair. In all experiments a minimum of 100 transients were averaged for each data point in order to boost the signal-to-noise ratio. The experiment's control software randomly ordered the different field strengths or directions so as to prevent any systematic distortion of the data by long-term drift, for example from sample photo-bleaching. The transient absorption signals (ΔA) were obtained with higher signal-to-noise than the corresponding magnetic field effects ($\Delta\Delta A$) which were more significantly affected by the shot-to-shot stability of the light sources

Results and Discussion

The transient absorption data in Figure 2 depict the effect of a static magnetic field on the recombination of the radical pair $[C^{\bullet+}PF^{\bullet-}]$ at 118 K. The figure displays the difference between the absorbance signals ($\Delta\Delta A(B_0)$) recorded in the presence, $\Delta A(B_0)$, and absence, $\Delta A(0)$, of the static magnetic field, B_0, as a function of the time, t, elapsed after the laser pulse. As observed previously, at early times ($t < 300$ ns) there is a change in the sign of the signal at ~1 mT.[17, 31] This phenomenon giving a maximum in the radical signal at around 0.5 mT is known as the 'Low Field Effect' and occurs only if the radical pair is sufficiently long-lived.[32, 33] However, a more unusual feature dominates the spectrum, namely the biphasic time-dependence of the signal observed at all field strengths. Using a simplified high-field model for the energy levels of the radical pair and the kinetic scheme shown in Figure 1B[31] we recently demonstrated that this time-inversion is due to the interplay of two important factors: (i) unusually, not all radical pairs are generated in the same initial spin state; 93% are formed in the singlet state, the other 7%, however, are triplet-born, (ii) at approximately 120 K, recombination from the singlet state with rate constant k_S is many times faster than any relaxation processes and also the recombination from the triplet state with rate constant k_T, i.e., $k_S \gg k_T$.[31] The latter observation is in contrast to previous studies conducted at 77 K and 292 K which found triplet recombination to be the dominant reaction pathway.[34] However, the relative energies of the radical pair and the triplet recombination product ^{3}CPF are a function of the solvent's relative permittivity which, for MeTHF, has been shown to change dramatically across this temperature range, in agreement with the trend in the rate constants.[31]

This interpretation of the time-inversion feature is further supported by transient EPR measurements used to probe in more detail the spin-polarization of the photogenerated radical pair. FIDs are obtained as a function of time (τ_1) after the laser trigger. Representative frequency-domain spectra are displayed in Figure 3A, with their integrals plotted as blue circles in Figure 3B. In the high fields (300 mT) employed here the energy-level diagram of Figure 1B aids interpretation of the observed effects: the $T_{+/-}$ states which are characterised by a non-zero magnetic moment along the field direction are energetically isolated from the two central states which are linear combinations of S and T_0 and hence independent of applied magnetic fields. As relaxation between the central states and $T_{+/-}$ has been shown to be slow ($< 10^5$ s^{-1})[31] it is obvious that creation of the radical pair in a pure singlet state would lead to an EPR signal whose intensity monotonically decreased with increasing τ_1 as the radicals recombined. The observation of a phase change at approximately 300 ns after the laser pulse and the subsequent temporal evolution of the spectra must be ascribed to (i) an initial population in the energetically isolated $T_{+/-}$ states which (ii) decays more slowly than the population from the central states. In agreement with the statements above, the EPR data confirm that $k_S \gg k_T$. As shown by the comparison in Figure 3B, this result is in excellent agreement with data we obtained previously using an X-band pulsed EPR inversion technique[31] in which the detection of the FID was preceded by a π inversion pulse. Using the FID at $\tau_1 < 0$ as a reference level the signal was found to decay

approximately exponentially as a function of the delay between the laser pulse and the π inversion pulse (again changing sign at 300 ns). Here we wish to highlight that as the radical pair is weakly coupled and the strength of the microwave field is small with respect to the width of the hyperfine spectrum of the radical pair the two radicals are not excited simultaneously. The net result of the π pulse is therefore to transfer all S/T_0 polarization to the $T_{\pm}$ states and *vice versa*. (double quantum beats are not observed).[35-37] At early times the signal is thus dominated by the initial singlet population and at late times by the initial triplet population with relative contributions of 93% and 7% as mentioned above. As $k_S \gg k_T$ the decay rate of the signal, k_d, can be related to the recombination rate from the singlet radical pair, k_S, through $k_S = 2 \times k_d = 1.8\times10^7\ s^{-1}$ (ref 31).

Returning to the low-field regime, Figure 4 depicts the change in radical absorbance, $\Delta\Delta A(B_0, B_1) = \Delta A(B_0, B_1) - \Delta A(B_0, 0)$, produced by a radiofrequency field of strength B_1 and frequency $\nu_{rf} = 36$ MHz when applied perpendicular to a static magnetic field ($B_0 = 0 - 4$ mT). As before, $\Delta\Delta A(B_0, B_1)$ is shown as a function of the time after the laser flash. The two distinct resonance features observed are both centred at $B_0 \sim 1.3$ mT (corresponding to the conventional EPR resonance condition, $\nu_{rf} = g_e\mu_B B_0/h$) but are characterised by very different linewidths. This feature is displayed even more dramatically in Figure 5A which provides a snapshot of the LF-RYDMR data obtained for both parallel and perpendicular orientations of static and RF fields, averaged from 750 to 850 ns after the laser pulse. It is obvious that in contrast to the spectra obtained in the perpendicular orientation, the data collected in the parallel mode display only the broad resonance feature. Moreover, in agreement with the time-resolved data for the static magnetic field effect in Figure 2 and the EPR data in Figure 3, the time-resolved LF-RYDMR spectra also display the expected biphasic time-dependence (and zero-crossing at approx. 300 ns), Figures 4 and 6A. [Data for parallel orientation of the fields is given in the ESI†]

Simple, brute force Liouville-space simulations (Figures 5B and 6B) of the LF-RYDMR data were performed using the previously described method,[31] with a singlet recombination rate constant, $k_S = 1.8 \times 10^7\ s^{-1}$ and an initial triplet population. $\lambda \approx 0.07$. Both parameters were determined prior to the simulations using the inversion experiment described above and in ref. [31]. The relaxation rate was a fitting parameter obtained as $2.1 \times 10^6\ s^{-1}$ in satisfactory agreement with our previous simulations of the MARY spectrum for which the relaxation rate was found to be $3.5 - 7.1 \times 10^5\ s^{-1}$ at 123 K and 4 mT. As it has been verified that $k_S \gg k_T$,[31] the recombination from the triplet state was assumed to be negligible ($k_T = 0$). Simulations included just two spin-1/2 nuclei in an attempt to reduce the number of variable parameters: the hyperfine couplings of the fullerene radical are small (< 100 μT) and hence were neglected while those of the carotenoid radical were represented by two ^{1}H couplings, both of 0.6 mT

Concentrating on the time-resolved RYDMR data (Figure 6), the Liouville simulations are in gratifyingly close agreement with the experimental data: (i) the phase change at approx. 300 ns is well reproduced and its origin has been discussed in detail above; (ii) the intensity of the signal increases with the amplitude of the oscillating field employed clearly indicating that the spin-locking regime[19, 22] is not reached for this radical pair even for the high-amplitude RF fields employed here; and (iii) even the very subtle delay in the occurrence of the zero-crossing with decreasing radiofrequency field strength is reproduced as larger RF fields lead to more efficient and rapid singlet-triplet interconversion. The simulations are surprisingly insensitive to the hyperfine couplings chosen [see ESI†] but instead show exceptional sensitivity to the rates of recombination and relaxation. The origin of this behaviour can be discovered by a re-examination of Figure 5. The experimental (Figure 5A) LF-RYDMR spectrum in the perpendicular orientation displays one broad and one narrow component which are easily assigned to the hyperfine-rich carotenoid radical (effective hyperfine coupling $a_{eff} = 0.988$ mT from DFT calculations[17]) and the almost hyperfine-devoid fullerene radical, respectively. In contrast, application of the static field parallel to the RF field results in a featureless broad signal entirely due to the carotenoid moiety. This general behaviour is reproduced in the simulation (Figure 5B) although resolved shoulders are observed which would have been considerably broader had a greater number of hyperfine couplings been included in the first radical. This unusual observation of a resonant feature for parallel fields may be rationalised using a simple two-spin model in which a single electron is coupled to a single $I = 1/2$ nucleus with hyperfine coupling a. For this spin system the only allowed electron spin-flip for parallel oscillating and static fields has a transition probability containing a factor $f = a/(B_0^2 + a^2)^{1/2}$.[38] In the high field regime when $B_0 \gg a$ this factor becomes negligible and transitions when the two fields are parallel are effectively forbidden, whereas such transitions become (partially) allowed when the hyperfine coupling and the static field strength are of similar magnitude. Returning to Figure 5, it is now obvious why the signal in the parallel case is entirely due to the carotenoid radical cation with its broad hyperfine spectrum ($B_0 \approx a$) whereas the sharp fullerene signal is observed only for the perpendicular orientation ($B_0 \gg a$). It is therefore obvious that the high-field selection rules typically employed in magnetic resonance (including X-band RYDMR) break down under the conditions employed here. However, they do so most dramatically for the carotenoid radical as its hyperfine couplings are of the same order of magnitude as the applied static magnetic field. This is an interesting result: the reaction yield probed in the LF-RYDMR experiment is determined by the concerted spin-evolution of the pair of radicals, yet the high-field approximation is clearly entirely invalid for one of the radicals whilst well-describing the field-response of the other. The origin of this observation lies in the fact that the radicals have a negligible mutual interaction so that the resonance frequencies of each radical are independent of the identity of its partner. However, spin-correlation lies at the heart of the RYDMR effect and it is the concerted spin-evolution of the two radicals that determines the relative and absolute intensities of the resonance signals.

Armed with this knowledge it is now possible to comprehend why, in the simulations, the hyperfine coupling parameters chosen for the carotenoid have such a minor effect on the time-resolved LF-RYDMR spectra of Figure 6B: the experiment is conducted at fields corresponding to the resonance condition for typical carbon-centred radicals (such as the fullerene and

carotenoid radicals) with $g \approx 2$ (ν_{rf} = 36 MHz and B_0 = 1.28 mT). The sharp resonance feature of the hyperfine-devoid fullerene radical has its highest intensity at this position whilst the resonance of the carotenoid is broadened significantly by its hyperfine couplings leading to a comparatively weaker contribution. Consequently, LF-RYDMR spectra can be satisfactorily simulated as long as one radical has no (or very small) hyperfine couplings (modelling the fullerene radical anion) whilst its partner has hyperfine couplings that broaden its spectrum significantly (modelling the carotenoid radical cation).

EPR data provide further insight into the different spectral characteristics of the two radicals. For measurements at X-band frequencies (~9 GHz), conducted as usual in the perpendicular mode, Fourier transformation of the FIDs results in spectra which lack the broad component but display a sharp resonance feature, Figure 3A. The integrated intensity of these spectra decays (as governed by the radical pair recombination) with the delay between the laser flash and the recording of the FID, Figure 3B. In analogy with the LF-RYDMR data above, the sharp spectral component can clearly be assigned to the fullerene radical. The carotenoid radical, so prominent in all LF-RYDMR spectra independent of the orientation of the two fields, on the other hand, is missing.

This observation is likely to be due to the interplay of three factors: (i) failure to irradiate the full hyperfine spectrum of the carotenoid radical results in a low intensity FID (ii) homogeneous broadening causes rapid (or complete) decay of the radical's modulations during the ~100 ns spectrometer dead time that follows the π/2 pulse and (iii) due to the carotenoid's broad hyperfine spectrum any remaining modulations will be low-frequency and thus difficult to discern within the observed tail of the FID. Nevertheless using a second microwave source in a pulsed ELDOR scheme (Figure 7A) it has been possible to observe both the fullerene radical anion and carotenoid radical cation, as shown in Figure 7B. The primary microwave channel is used to provide two hard pulses, an inversion pulse 200 ns after the laser flash, and a π/2 detection pulse at t = 2 μs, both acting on the fullerene radical anion. Shortly after the inversion pulse the secondary (ELDOR) microwave channel provides a 500 ns (~2.4 MHz full width at half maximum) soft pulse. This small tip-angle pulse projects some carotenoid radical magnetization into the transverse plane, perturbing the radical pair spin state and therefore altering the FID observed from the fullerene radical anion. Sweeping the frequency of the selective ELDOR pulse therefore maps out a frequency-domain spectrum of the radical pair. Using low power (highly attenuated) pulses in the ELDOR channel only a sharp signal arising from the fullerene anion is observed, whereas at higher powers a second broad resonance becomes apparent centred at around 9.69 GHz, corresponding to the carotenoid radical cation. As expected from the previously reported electron g-values[30] the carotenoid signal is centred at a higher frequency that the fullerene signal, confirming the assignment.

Finally, the full angle- and time-dependence of the LF-RYDMR signal is explored in Figure 8A, for a static field B_0 = 1.28 mT rotated relative to an oscillating field ν_{rf} = 36 MHz, B_1 = 0.17 mT. To allow comparison of different RF field strengths we average the data over the 850 to 950 ns time window, Figure 9A, finding that the angular variation of the broad negative signal close to the perpendicular alignment (θ = 90°, 270°) broadens with B_1. This behaviour is again satisfactorily reproduced in Liouville-space simulations, Figure 9B. Overestimation of the relative signal intensity for the parallel alignment is attributed to the small number of hyperfine couplings included in the simulations. By simple transition probability arguments it becomes apparent that power broadening of the sharp signal is the likely origin of the broadening of the angular dependence. Extending this argument Liouville-space rotary-RYDMR simulations have been performed in which the oscillating field term is removed from the spin-Hamiltonian and the effect of this field instead included in the relaxation superoperator for the fullerene radical anion as an additional Fermi golden rule transition probability. The rate constant of the RF induced transition can be written as,

$$k_{RF} = \frac{2\pi}{\hbar}\left|\langle f|H|i\rangle\right|^2 \boldsymbol{\rho}$$

where,

$$\langle f|H|i\rangle = \langle \boldsymbol{\beta}|g\boldsymbol{\mu}_B B_1 S_X|\boldsymbol{\alpha}\rangle \sin\boldsymbol{\theta} = \frac{g\boldsymbol{\mu}_B B_1}{2}\sin\boldsymbol{\theta}$$

assuming that the RF-induced transition only flips the electron spin of the fullerene radical (at resonance the contribution from the fullerene radical is dominant because that from the carotenoid is distributed over a much wider static field range by the many hyperfine splittings). The state density ρ is approximated by the inverse of the linewidth ($\Delta B \approx 0.6$ mT) according to,

$$\boldsymbol{\rho} \cong \frac{1}{g\boldsymbol{\mu}_B \Delta B}.$$

Finally, the RF term in the spin-Hamiltonian is omitted, and the relaxation superoperator modified to include an effective spin-lattice relaxation rate,

$$\left(\frac{1}{T_1}\right)_{eff} = \frac{1}{T_1} + 2k_{RF}.$$

The resulting simulations shown in Figure 8B alongside conventional calculations, Figure 8C, satisfactorily reproduce the experimental data including the signal-inversion without the need for an explicit consideration of the time-dependent radiofrequency field. The time-dependent spectra thus arise mainly from radical pair recombination kinetics modulated by an incoherent RF-induced population transfer.

We have provided experimental evidence for the breakdown of high-field selection rules in the low-frequency limit, yet have verified that relatively simple models can be used to understand this behaviour. The frequency of the oscillating field employed in our RYDMR experiments is still many times greater than that used in previously reported animal behavioural studies exploring the hypothesis of radical pair based magnetoreception in European robins,[4-6] yet we can begin to provide insight into those experimental observations. It was reported that parallel static and oscillating fields do not disrupt the magnetic orientation of the birds but that at an angle of θ = 24° disorientation does occur.[5, 6] If the effect of varying the angle between the fields followed a

simple squared sinusoidal dependence as would be expected at high field then the RYDMR signal for this angle would be less than 17% of that expected for the fully allowed perpendicular alignment, with $\theta = 0°$ giving no RYDMR signal at all. Our results demonstrate experimentally that quite different behaviour can be seen in the low-frequency regime with both parallel and perpendicular alignments giving broad RYDMR signals. Only the narrow feature from a radical devoid of hyperfine couplings was observed to show a significant angular variation as expected at high-field (Figure 5), and broadening of this narrow resonance feature by an increase in the oscillating field strength led to a much sharper transition between these two extremes for small values of θ (Figure 9). The observation that variation in the angle between the 46 μT geomagnetic field and an on-resonance 1.315 MHz RF field between only 0° and 24° could disturb compass orientation of birds[6] is therefore less perplexing than it at first appears. One radical will contribute a RYDMR signal of roughly the same intensity independent of the orientation of the magnetic fields which is clearly insufficient in magnitude to cause migratory disorientation, but in addition to this a strongly orientation dependent response arises from a radical with narrow hyperfine spectrum which with only a small angular variation is able to tip the balance to migratory disorientation. Nevertheless, the earlier report of the same angle dependence for an off-resonance 7 MHz RF field is surprising,[5] such an experiment probing only the broad off-resonance signal that we have found to be insensitive to field orientation (Figure 5).

Our results suggest that at resonance a more significant difference will be seen between the LF-RYDMR signals for parallel and perpendicular orientations if one of the radicals has a narrow hyperfine spectrum. Recent work has predicted the increased compass sensitivity to a ~50 μT static field of systems in which one radical has no significant hyperfine interactions, and even suggested the possible identity of such a radical pair in cryptochrome.[12] It would therefore be interesting to explore how the threshold RF field strength for disorientation of migratory birds varies depending on the angle between static and RF fields. Previous work which identified a 15 nT threshold at 1.315 MHz used a 24° angle between static and RF fields[4]. Moving closer to perpendicular alignment a stronger RYDMR effect and hence lower-threshold field is expected if one of the radicals involved has a hyperfine spectrum that is narrow with respect to the static field strength. The orientation dependence of the threshold field could therefore: (i) verify the assertion that one radical is almost devoid of hyperfine couplings, (ii) indicate the actual width of the narrow hyperfine spectrum through the strength of the orientation dependence, and (iii) identify the true RF sensitivity threshold which for perpendicular alignment could be lower than the reported 15 nT value.

Conclusions

We have presented time-resolved LF-RYDMR spectra of a model system for a radical-pair-based avian magnetoreceptor, demonstrating the way in which the strengths and relative orientation of static and oscillating magnetic fields, recombination and relaxation kinetics and hyperfine couplings all interplay to determine the overall spectral response. Nevertheless, we are able to reproduce this complex behaviour in simulations using a minimal number of variable parameters, as described above. It has been experimentally verified that the effect of varying the angle between the static and oscillating fields is crucially dependent on the magnitude of hyperfine couplings relative to the static field strength. It is hence of crucial importance to consider this factor when attempting to interpret *in vivo* animal studies which have previously used very weak (46 μT) static fields.[4-6]

Acknowledgements

The authors are grateful for the financial support of this work from DARPA (QuBE: N66001-10-1-4061), the Engineering and Physical Research Council and the EMF Biological Research Trust. We thank Neville Baker for construction of the RF circuit and Dr Kevin Henbest for many useful discussions.

Notes and references

[a] *Department of Chemistry, University of Oxford, Centre for Advanced Electron Spin Resonance, Inorganic Chemistry Laboratory, Oxford, OX1 3QR, UK.*
E-mail: christiane.timmel@chem.ox.ac.uk
[b] *Present Address: Department of Chemistry, Graduate School of Science and Engineering, Saitama University, Shimo-okubo, Sakura-ku, Saitama 338-8570, Japan.*
[c] *Department of Chemistry and Biochemistry, Arizona State University, Tempe, Arizona, USA.*
[d] *Department of Chemistry, University of Oxford, Physical & Theoretical Chemistry Laboratory, Oxford, OX1 3QZ, UK.*
[e] *Department of Physics, University of Warwick, Gibbet Hill Road, Coventry, CV4 7AL, UK.*
E-mail: c.wedge@warwick.ac.uk
[‡] *These authors contributed equally.*

† Electronic Supplementary Information (ESI) available: Additional experimental data, details of data processing, additional experimental details, field orientation diagram and stability tests of simulation DOI: 10.1039/b000000x/

1. K. Schulten, C. E. Swenberg and A. Weller, *Z. Phys. Chem. Neue. Fol.*, 1978, **111**, 1-5.
2. H. Mouritsen and P. J. Hore, *Curr. Opin. Neurobiol.*, 2012, **22**, 343-352. 10.1016/j.conb.2012.01.005
3. C. T. Rodgers and P. J. Hore, *Proc. Natl. Acad. Sci.*, 2009, **106**, 353-360. 10.1073/pnas.0711968106
4. T. Ritz, R. Wiltschko, P. J. Hore, C. T. Rodgers, K. Stapput, P. Thalau, C. R. Timmel and W. Wiltschko, *Biophys. J.*, 2009, **96**, 3451-3457. 10.1016/j.bpj.2008.11.072
5. T. Ritz, P. Thalau, J. B. Phillips, R. Wiltschko and W. Wiltschko, *Nature*, 2004, **429**, 177-180. 10.1038/Nature02534
6. P. Thalau, T. Ritz, K. Stapput, R. Wiltschko and W. Wiltschko, *Naturwissenschaften*, 2005, **92**, 86-90. 10.1007/s00114-004-0595-8
7. T. Biskup, *Mol. Phys.*, 2013, **111**, 3698-3703. 10.1080/00268976.2013.833350
8. E. W. Evans, C. A. Dodson, K. Maeda, T. Biskup, C. J. Wedge and C. R. Timmel, *Interface Focus*, 2013, **3**, 20130037. 10.1098/rsfs.2013.0037 2042-8901
9. H. J. Hogben, T. Biskup and P. J. Hore, *Phys. Rev. Lett.*, 2012, **109**, 220501.
10. J. C. S. Lau, C. T. Rodgers and P. J. Hore, *J. R. Soc. Interface*, 2012, **9**, 3329-3337. 10.1098/rsif.2012.0374
11. J. C. S. Lau, N. Wagner-Rundell, C. T. Rodgers, N. J. B. Green and P. J. Hore, *J. R. Soc. Interface*, 2010, **7**, S257-S264. 10.1098/rsif.2009.0399.focus

12. A. A. Lee, J. C. S. Lau, H. J. Hogben, T. Biskup, D. R. Kattnig and P. J. Hore, *J. R. Soc. Interface*, 2014, **11**, 20131063. 10.1098/rsif.2013.1063
13. T. Ritz, S. Adem and K. Schulten, *Biophys. J.*, 2000, **78**, 707-718.
14. C. A. Dodson, P. J. Hore and M. I. Wallace, *TIBS*, 2013, **38**, 435-446. 10.1016/j.tibs.2013.07.002
15. K. Maeda, A. J. Robinson, K. B. Henbest, H. J. Hogben, T. Biskup, M. Ahmad, E. Schleicher, S. Weber, C. R. Timmel and P. J. Hore, *Proc. Natl. Acad. Sci.*, 2012, **109**, 4774-4779. 10.1073/pnas.1118959109
16. G. Kodis, P. A. Liddell, A. L. Moore, T. A. Moore and D. Gust, *J. Phys. Org. Chem.*, 2004, **17**, 724-734. 10.1002/Poc.787
17. K. Maeda, K. B. Henbest, F. Cintolesi, I. Kuprov, C. T. Rodgers, P. A. Liddell, D. Gust, C. R. Timmel and P. J. Hore, *Nature*, 2008, **453**, 387-390. 10.1038/Nature06834
18. K. B. Henbest, P. Kukura, C. T. Rodgers, P. J. Hore and C. R. Timmel, *J. Am. Chem. Soc.*, 2004, **126**, 8102-8103. 10.1021/Ja048220q
19. C. J. Wedge, J. C. S. Lau, K.-A. Ferguson, S. A. Norman, P. J. Hore and C. R. Timmel, *Phys. Chem. Chem. Phys.*, 2013, **15**, 16043-16053. 10.1039/C3CP52019F
20. S. Engels, N.-L. Schneider, N. Lefeldt, C. M. Hein, M. Zapka, A. Michalik, D. Elbers, A. Kittel, P. J. Hore and H. Mouritsen, *Nature*, 2014, **509**, 353-356. 10.1038/nature13290
21. U. E. Steiner and T. Ulrich, *Chem. Rev.*, 1989, **89**, 51-147.
22. S. N. Batchelor, K. A. McLauchlan and I. A. Shkrob, *Mol. Phys.*, 1992, **75**, 501-529.
23. S. N. Batchelor, K. A. McLauchlan and I. A. Shkrob, *Mol. Phys.*, 1992, **75**, 531-561.
24. M. K. Bowman, D. E. Budil, G. L. Closs, A. G. Kostka, C. A. Wraight and J. R. Norris, *Proc. Natl. Acad. Sci.*, 1981, **78**, 3305-3307.
25. K. Enjo, K. Maeda, H. Murai, T. Azumi and Y. Tanimoto, *J. Phys. Chem. B*, 1997, **101**, 10661-10665.
26. C. T. Rodgers, K. B. Henbest, P. Kukura, C. R. Timmel and P. J. Hore, *J. Phys. Chem. A*, 2005, **109**, 5035-5041. 10.1021/Jp050765z
27. C. J. Wedge, C. T. Rodgers, S. A. Norman, N. Baker, K. Maeda, K. B. Henbest, C. R. Timmel and P. J. Hore, *Phys. Chem. Chem. Phys.*, 2009, **11**, 6573-6579. 10.1039/B907915g
28. J. R. Woodward, C. R. Timmel, P. J. Hore and K. A. McLauchlan, *Mol. Phys.*, 2002, **100**, 1181-1186. 10.1080/00268970110109961
29. C. T. Rodgers, C. J. Wedge, S. A. Norman, P. Kukura, K. Nelson, N. Baker, K. Maeda, K. B. Henbest, P. J. Hore and C. R. Timmel, *Phys. Chem. Chem. Phys.*, 2009, **11**, 6569-6572. 10.1039/B906102a
30. M. Di Valentin, A. Bisol, G. Agostini and D. Carbonera, *J. Chem. Inf. Mod.*, 2005, **45**, 1580-1588. 10.1021/ci050183e
31. K. Maeda, C. J. Wedge, J. G. Storey, K. B. Henbest, P. A. Liddell, G. Kodis, D. Gust, P. J. Hore and C. R. Timmel, *Chem. Commun.*, 2011, **47**, 6563-6565. 10.1039/C1cc11625h
32. U. Till, C. R. Timmel, B. Brocklehurst and P. J. Hore, *Chem. Phys. Lett.*, 1998, **298**, 7-14. 10.1016/S0009-2614(98)01158-0
33. C. R. Timmel, U. Till, B. Brocklehurst, K. A. McLauchlan and P. J. Hore, *Mol. Phys.*, 1998, **95**, 71-89. 10.1080/00268979809483134
34. D. Kuciauskas, P. A. Liddell, A. L. Moore, T. A. Moore and D. Gust, *J. Am. Chem. Soc.*, 1998, **120**, 10880-10886.
35. V. R. Gorelik, K. Maeda, H. Yashiro and H. Murai, *J. Phys. Chem. A*, 2001, **105**, 8011-8017. 10.1021/Jp0109628
36. K. M. Salikhov and Y. N. Molin, *J. Phys. Chem.*, 1993, **97**, 13259-13266. 10.1021/J100152a033
37. Y. Araki, K. Maeda and H. Murai, *Chem. Phys. Lett.*, 2000, **332**, 515-520. 10.1016/S0009-2614(00)01291-4
38. A. Carrington and A. D. McLachlan, *Introduction to magnetic resonance : with applications to chemistry and chemical physics*, Chapman and Hall, London, 1979.

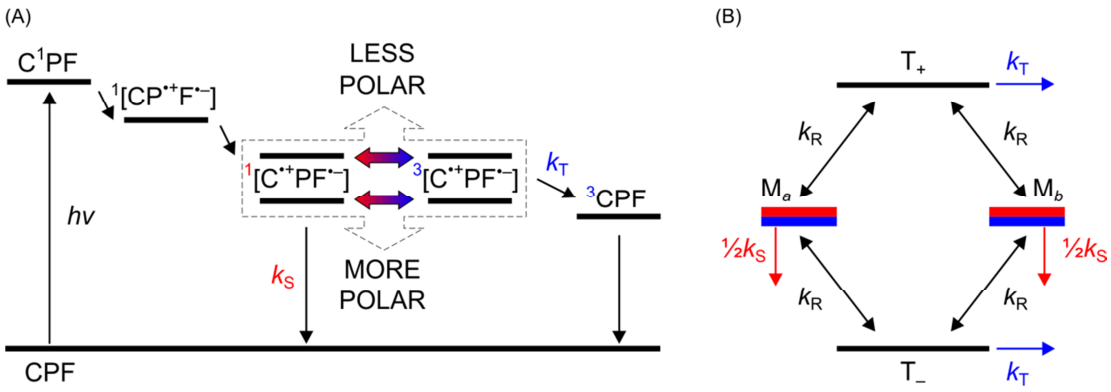

Figure 1. (A) Photochemistry of the CPF triad. The energy of the charge-separated state is strongly dependent upon the polarity of the solvent, with a more polar environment strongly favouring singlet recombination (Marcus inverted region) over triplet recombination (Marcus normal region). (B) Electron spin states of a radical pair under high field conditions (applied magnetic field much greater than the average hyperfine interaction within the radical pair). The thickness of the bars indicates the initial populations of the four states. $T_{\pm}$ recombine exclusively by triplet recombination whereas depopulation of the states $M_{a,b}$ which are linear combinations of S and T_0 is dominated by the much faster singlet recombination. The spin-relaxation pathways are labelled with the rate constant k_R.

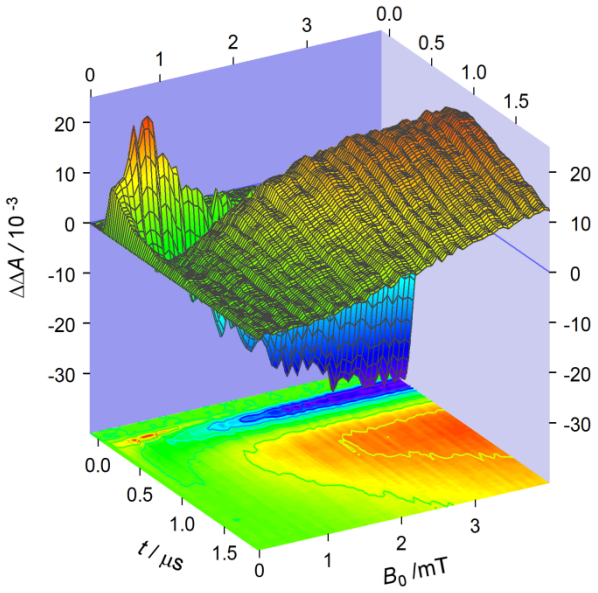

Figure 2. Time-resolved static MFE spectrum of the CPF triad in MeTHF solvent, at 118 K. Data were recorded by transient absorption with a monitoring wavelength of 975 nm.

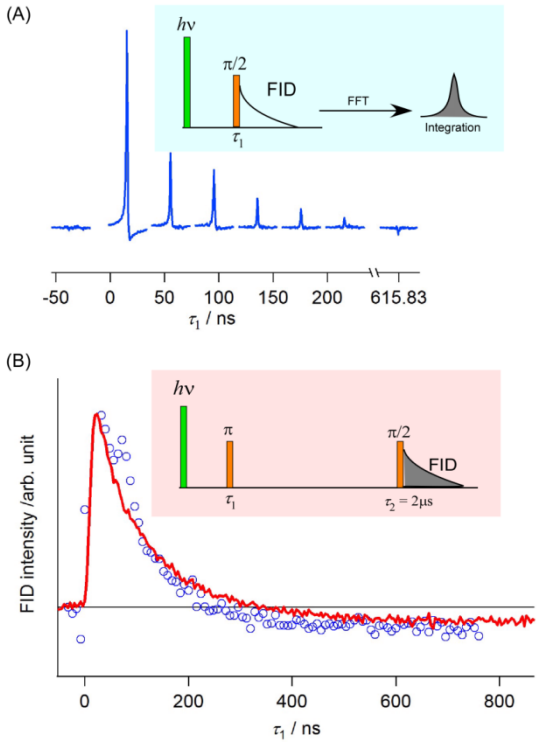

Figure 3. (A) Time-resolved Fourier transform 9.7 GHz EPR spectra of photo-excited CPF at various times relative to the laser pulse; the inset shows the pulse sequence employed. Inversion of spin-polarization is apparent in the obvious phase inversion at 300 ns after the laser pulse, though it should be noted that the absolute phase is arbitrary. The linewidths of the spectra are limited due to apodization with an exponential window function prior to Fourier transformation. Spectra were recorded at 110 K in MeTHF. (B) Time-dependence of the electron spin polarization observed, blue open circles for the pulse sequence shown as an inset in (A) in which the frequency-domain spectra are integrated and the red line for the inversion experiment, using the pulse sequence in the inset in (B) in which the time-domain FID is integrated directly. In both cases the time τ_1 between the laser flash and the first microwave pulse is varied.

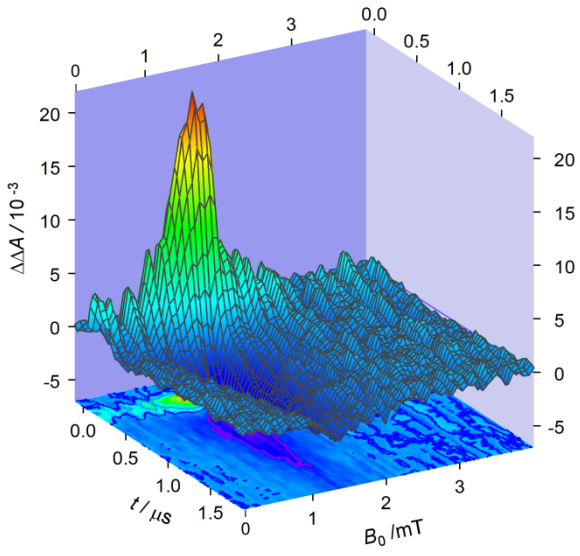

Figure 4. Time-resolved LF-RYDMR spectrum of the CPF triad in MeTHF with static field B_0 perpendicular to the oscillating field B_1 = 0.1 mT, ν_{rf}= 36 MHz. Other experimental conditions are as indicated in Figure 2.

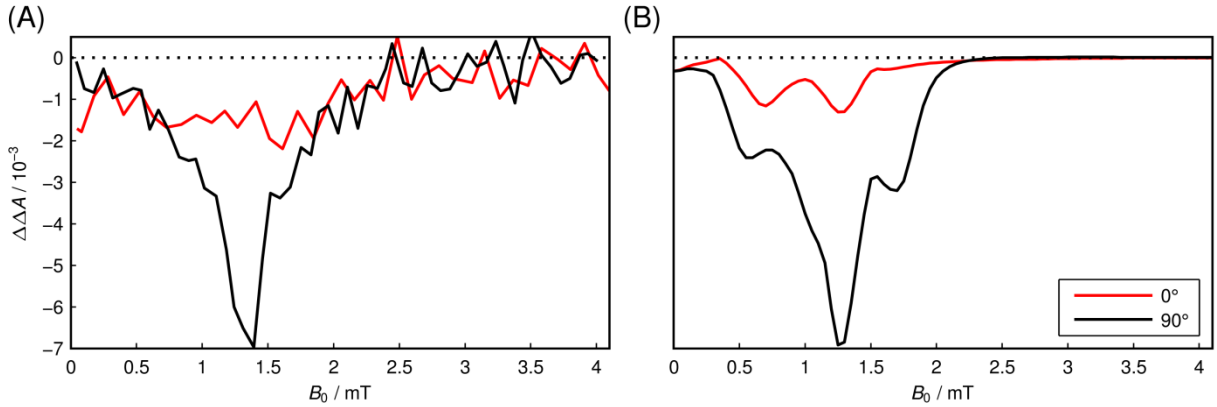

Figure 5. Comparison of LF-RYDMR spectra for parallel and perpendicular orientations of static and oscillating magnetic fields. In the perpendicular case a sharp resonance is observed centred at $B_0 \sim 1.3$ mT, along with a broader signal; only the broad signal is observed for parallel orientations. (A) Experimental data recorded for CPF at 118 K in MeTHF using time traces averaged from 750 to 850 ns; $B_1 = 0.1$ mT, $\nu_{rf} = 36$ MHz. (B) Simulated data generated using two electrons (both $S = 1/2$; $g_1 = 2.00271$, $g_2 = 2.00023$) and two nuclei ($I = 1/2$) with hyperfine couplings $a_3 = a_4 = 0.6$ mT (both on radical 1), $T_1 = T_2 = 1 \times 10^6$ s^{-1}, $k_S = 1.8 \times 10^7$ s^{-1}, and initial triplet fraction $\lambda = 0.07$.

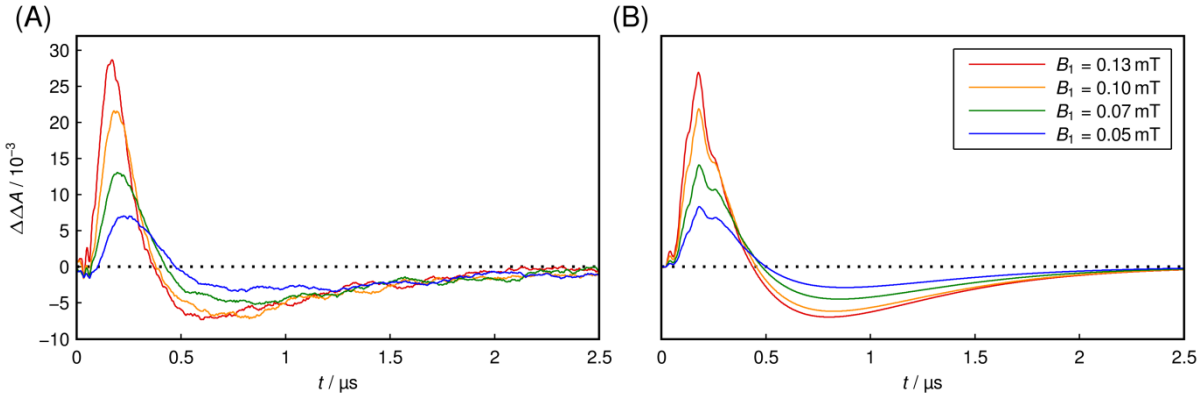

Figure 6. (A) Experimental LF-RYDMR data for CPF at 118 K following a 532 nm laser flash at time $t = 0$ for perpendicular orientations of static and oscillating fields. The data show the difference in transient absorption traces in the presence, $\Delta A(B_0, B_1)$ and absence $\Delta A(B_0, 0)$ of the 36 MHz oscillating field, with a $B_0 = 1.28$ mT static field applied in both cases. All traces have been filtered to remove 36 MHz interference as detailed in the ESI†. (B) Simulated time traces, parameters as for Figure 5B. Additional fine structure in (B) arises from inclusion of only a small number of hyperfine couplings in the simulation.

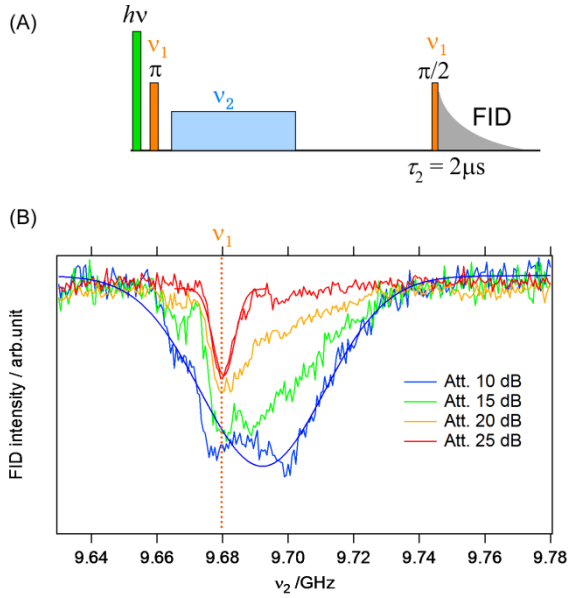

Figure 7. (A) Pulse scheme for the transient-EPR ELDOR experiment on the CPF triad. (B) The FID-detected ELDOR spectra observed at 110 K. Coloured lines are spectra recorded for various powers of the second microwave source (ν_2) as indicated by the source attenuation in the legend. For the ν_1 channel 16 ns pulses had a turning angle of $\pi/2$; the ν_2 pulse is 500 ns in length corresponding to an excitation bandwidth of ~2.4 MHz. Smooth curves are Gaussian fits to the red and blue spectra. Static field $B_0 = 344.8$ mT, main microwave frequency $\nu_1 = 9.675983$ GHz.

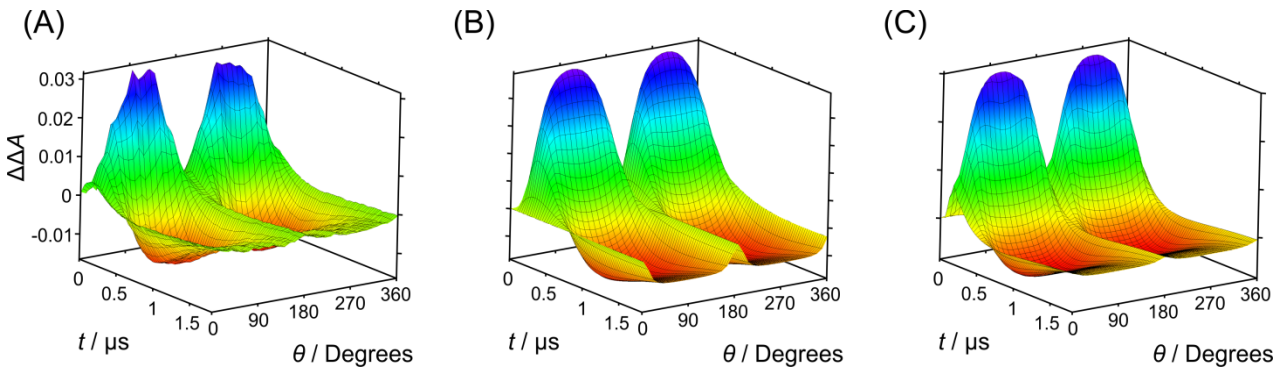

Figure 8 Rotary-RYDMR spectra of the CPF triad in MeTHF. (A) Experimental data obtained by transient absorption, recorded at 114 K with ν_{rf} = 36 MHz, B_1 = 0.17 mT and B_0 = 1.28 mT. Simulated rotary-RYDMR spectrum using (B) Fermi-golden rule transition probabilities and (C) conventional quantum mechanical treatment of the oscillating field (see text for details). Both simulations use the parameters given for Figure 5B.

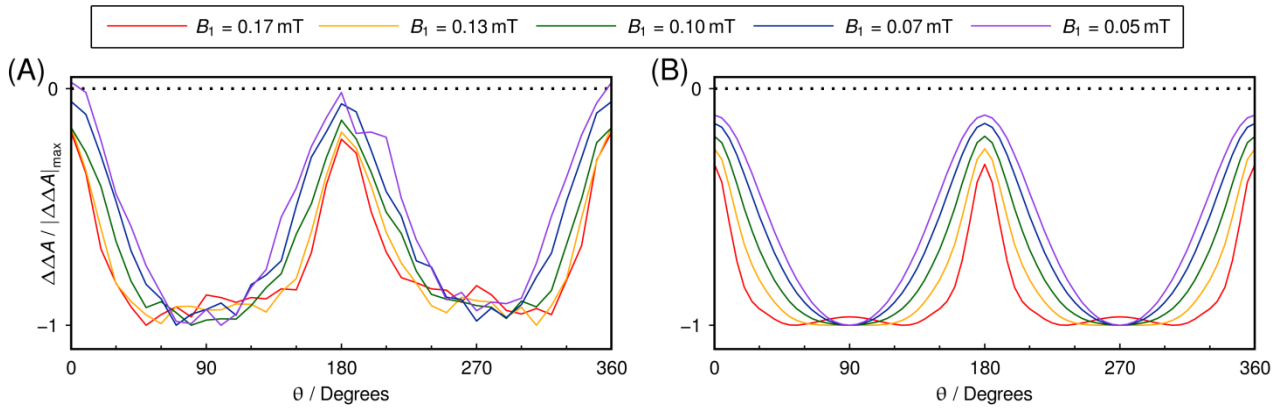

Figure 9. Rotary-RYDMR spectra of the CPF triad in MeTHF averaged between 850 and 950 ns after the excitation pulse. (A) Experimental spectra recorded at 118 K with ν_{rf} = 36 MHz and B_0 = 1.28 mT for a range of RF field strengths as indicated. (B) Simulated spectra using the parameters given for Figure 5B. In all cases spectra are scaled to have the same maximal negative signal intensity in order to aid comparison of the spectral widths.

Probing a Chemical Compass: Novel Variants of Low-Frequency Reaction Yield Detected Magnetic Resonance.

Supporting Information

Kiminori Maeda,[a,b,‡] Jonathan G. Storey,[a,‡] Paul A. Liddell,[c] Devens Gust,[c] P. J. Hore,[d] C. J. Wedge[e,*] and Christiane R. Timmel[a,*]

[a] Department of Chemistry, University of Oxford, Centre for Advanced Electron Spin Resonance, Inorganic Chemistry Laboratory, Oxford, OX1 3QR, UK.
Email: christiane.timmel@chem.ox.ac.uk

[b] Present Address: Department of Chemistry, Graduate School of Science and Engineering, Saitama University, Shimo-okubo, Sakura-ku, Saitama 338-8570, Japan.

[c] Department of Chemistry and Biochemistry, Arizona State University, Tempe, Arizona, USA.

[d] Department of Chemistry, University of Oxford, Physical & Theoretical Chemistry Laboratory, Oxford, OX1 3QZ, UK.

[e] Department of Physics, University of Warwick, Gibbet Hill Road, Coventry, CV4 7AL, UK.
Email: c.wedge@warwick.ac.uk

[‡] These authors contributed equally to this work

Contents

1. Filtering of time-profiles

Time-profiles in RYDMR experiments contained significant RF noise due to radiation from the high power RF circuits. For sufficiently short-lived radical pairs this can be filtered from the time-profile using a boxcar algorithm with gate-width equal to the RF period of 27.8 ns. However, the transient absorption signal of the CPF triad studied here decays over a few microseconds. This means that an observation window sufficiently long to capture the entire decay necessitates a lower time-resolution which insufficiently samples the RF noise for boxcar filtering to be effective. Experimental data were manipulated using two filters: i) a second order low-pass filter with a cut-off frequency of 50 MHz (−3dB). This filter removes high-frequency noise from the spectrum. The cut-off frequency was selected as Fourier transforms of the experimental signals show only a small component above 50 MHz. ii) A 36 MHz notch filter, with $Q = 2$. This sharp filter is used to remove the RF pick-up at 36 MHz, while leaving the rest of the signal intact. Multiple comparisons between filtered and raw data confirmed that no significant distortion of the time-profiles occurred using this method.

Simulated data do not suffer from RF pickup, and so were filtered with the low-pass filter alone, to allow for an accurate comparison between the simulated and experimental data.

2. Additional experimental details

2.1. RF circuit and timing control

In order to maximize the magnitude of the oscillating field and provide an impedance match for the RF amplifier, a tuned circuit is used with parallel and series trimming capacitors adjusted to give an overall load of 50 Ω. The pulsing of the RF is controlled by a home-built synchronisation unit which gates the input from a 36 MHz frequency source (PTS-200) and the 100 W RF amplifier (Wessex RC114-100) in response to a trigger signal. The timing of this unit is controlled by two Stanford delay generators (SRS DG535). The master delay generator provides the trigger source with a 10 Hz repetition rate, which in turn triggers the laser flash lamps with a TTL pulse. The second output is delayed by 200–300 μs, providing approximately the required Q-switch delay for the laser. This pulse arms the RF gating unit which is then triggered by the next positive-going transition of the RF input, causing the RF gate to open if the computer-controlled RF flag is high. A small additional delay is then applied to allow for the rise time of the RF amplifier before a TTL pulse output triggers the laser Q-switch. The RF gate-width is sufficient to allow complete decay of the RP signal before the gate is closed. As the gating unit controls both the RF gate and the laser trigger it is possible with this setup to control the initial phase of the RF field when the RP is generated. Although the 7 ns pulse of the laser corresponds to a significant fraction of one RF period at 36 MHz, this technology allows the effect of RF phase at the moment of RP generation to be investigated at lower frequencies [J.G. Storey *et al*., manuscript in preparation]. As the phase of the RF signal is fixed relative to the laser trigger the second delay generator is used to introduce a half period (13.885 ns) delay to half of the Q-switch trigger pulses with the effect of efficiently cancelling RF interference on the signal cables.

2.2. Relative field orientation

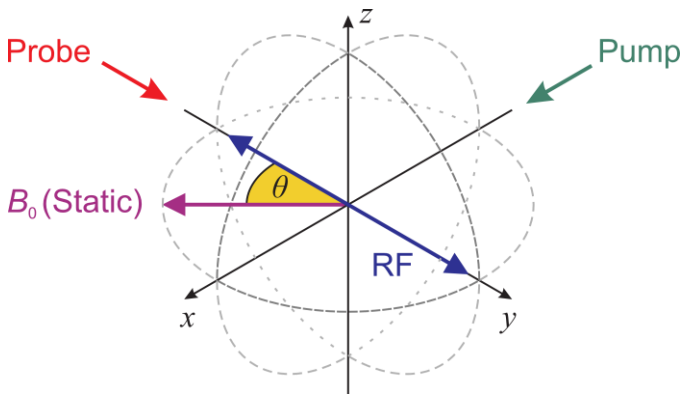

Figure S1. Relative orientations of optical excitation and magnetic fields for the RYDMR experiment, all of which lie in the horizontal plane. The pump pulse (532 nm) and probe beam (975 nm) are perpendicular, the radiofrequency oscillating field is linearly-polarised and co-linear with the probe beam. The static field direction is defined by the angle θ with respect to the RF field.

3. EPR data

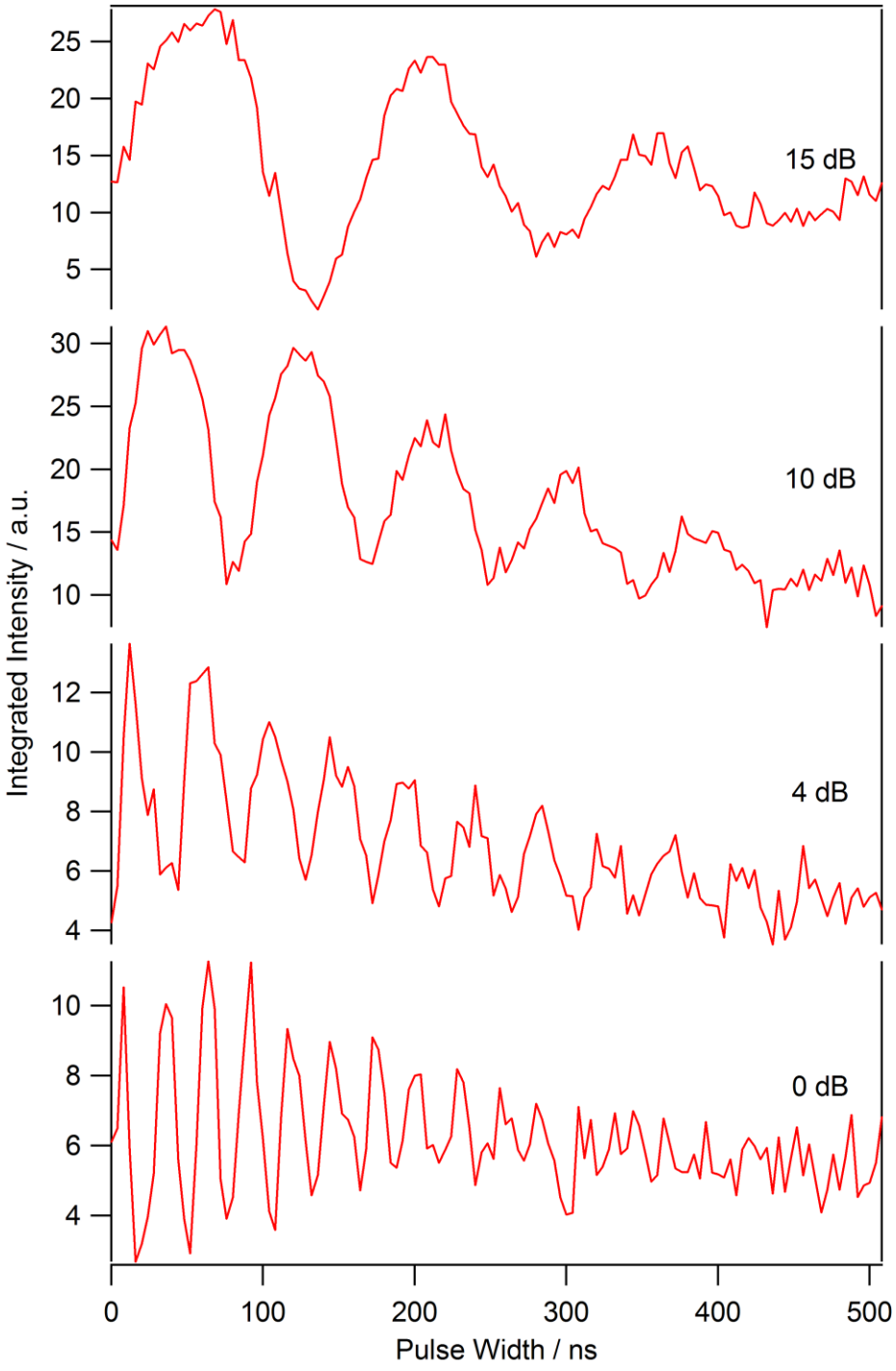

Figure S2. Transient-EPR nutation data for the CPF triad as a function of microwave attenuation. Data are presented as a function of the length of a microwave pulse applied 200 ns after the radical-generating 532 nm laser pulse. Detection is achieved by integrating the FID obtained from a π/2 pulse at a fixed time of 2 μs after the laser pulse. Experiments were performed at 110 K, B_0 = 347 mT, ν_{mw} = 9.686 GHz. Note that no double-frequency beats are observed.

4. RYDMR data

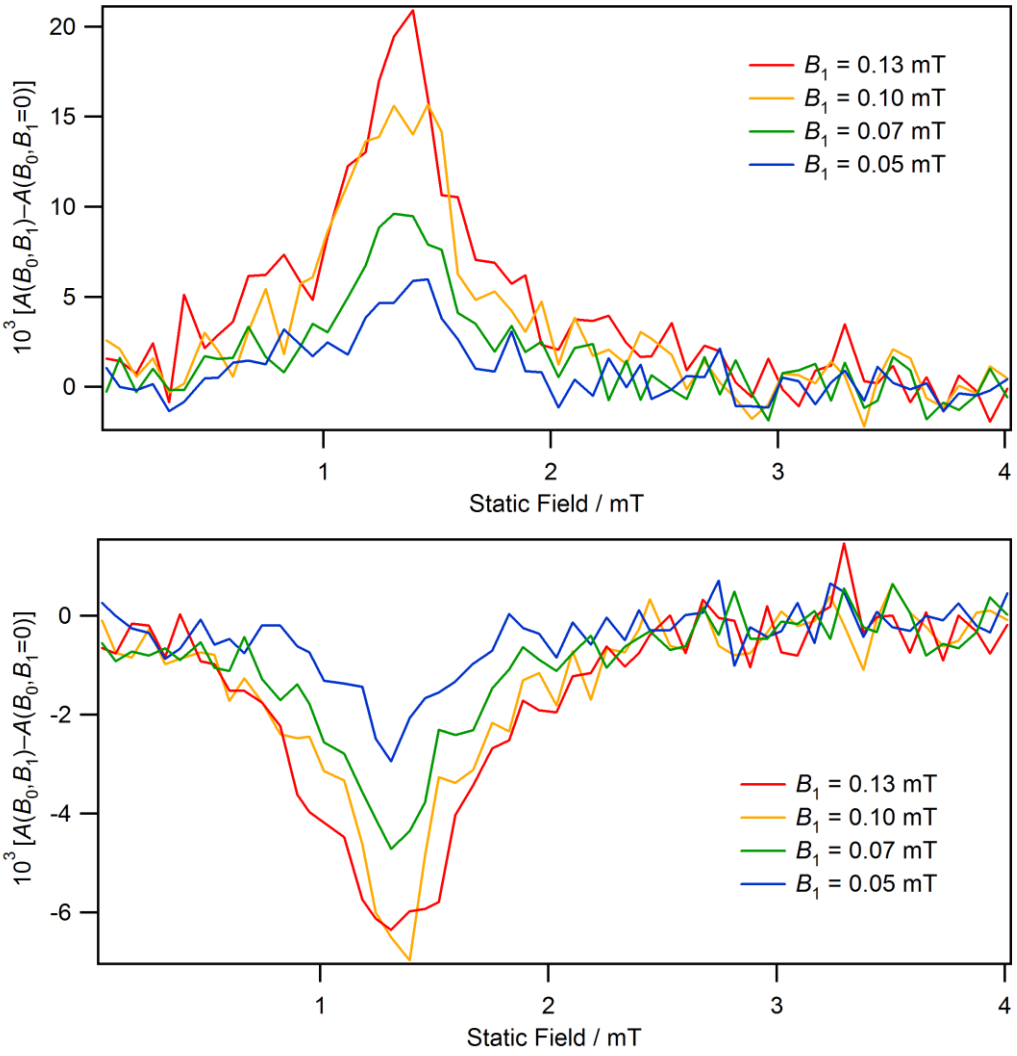

Figure S3. Time-resolved RYDMR spectra as a function of oscillating field strength as indicated. Spectra were recorded with perpendicular static and 36 MHz oscillating fields and are the result of averaging data over the range 100 to 300 ns (top) and 700 to 900 ns (bottom) after the laser flash, respectively.

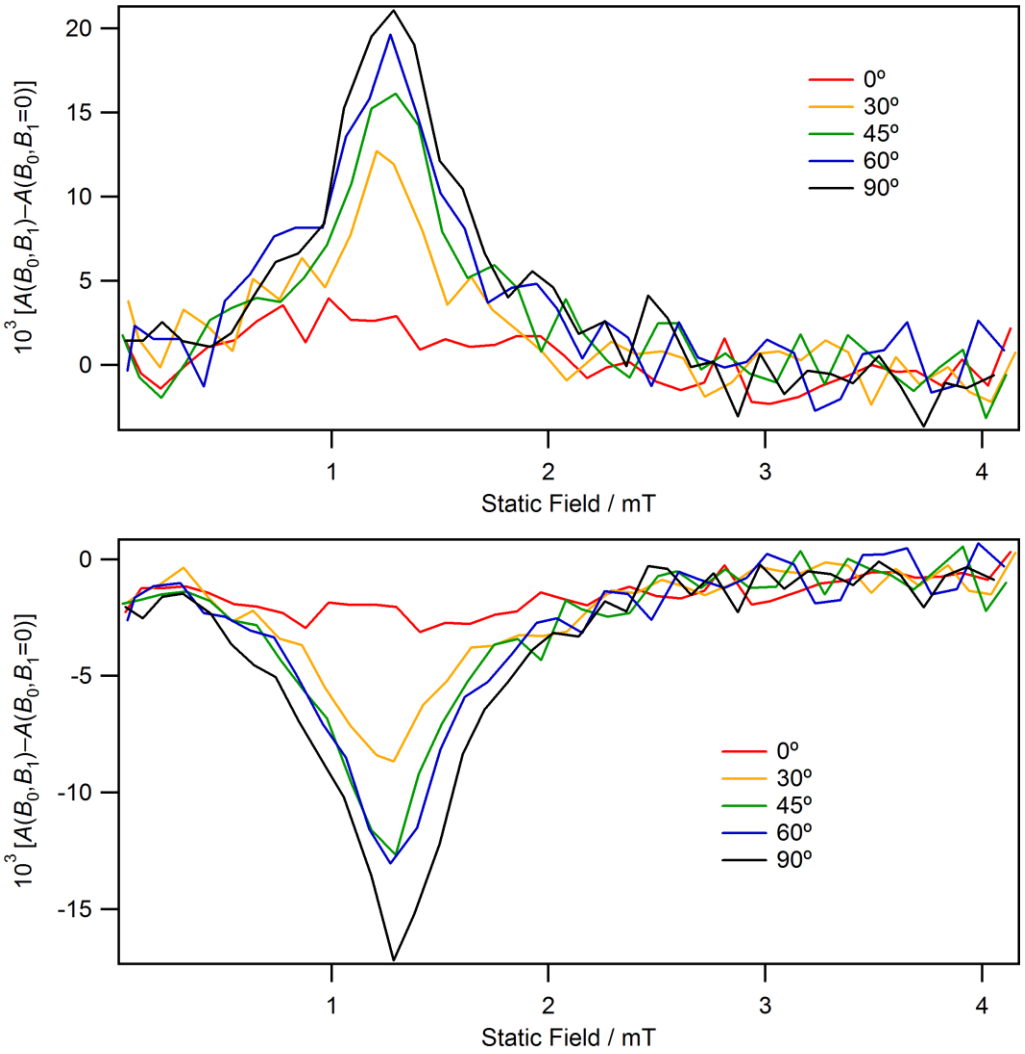

Figure S4. Time-resolved RYDMR spectra as a function of angle θ between the static and oscillating magnetic fields as indicated. Spectra are the result of averaging data over the range 100 to 300 ns (top) and 700 to 900 ns (bottom) after the laser flash, respectively. B_1 = 0.13 mT, ν_{rf} = 36 MHz.

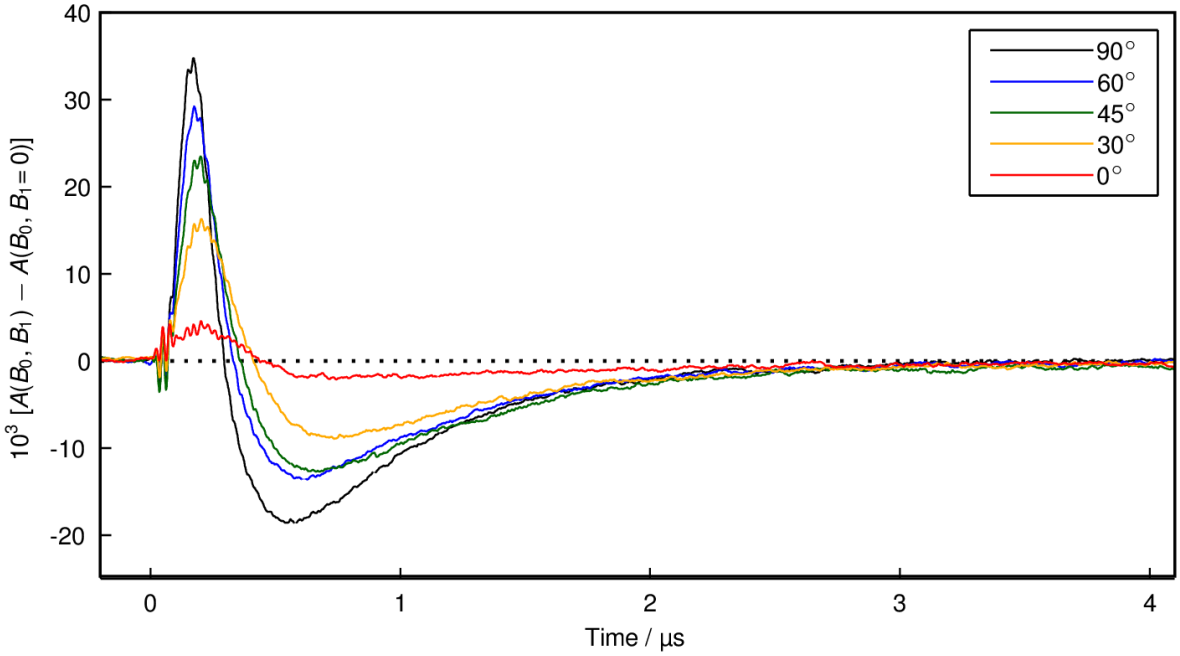

Figure S5. Transient-absorption detected RYDMR time-profiles as a function of angle θ between static and oscillating magnetic fields. In all cases a signal inversion can be observed corresponding to inversion of spin-polarization, with the time of this inversion moving to slightly later times as the fields are rotated away from perpendicular alignment which reduces the efficiency of the spin-mixing process. $B_0 = 1.28$ mT, $\nu_{rf} = 36$ MHz, $B_1 = 0.13$ mT.

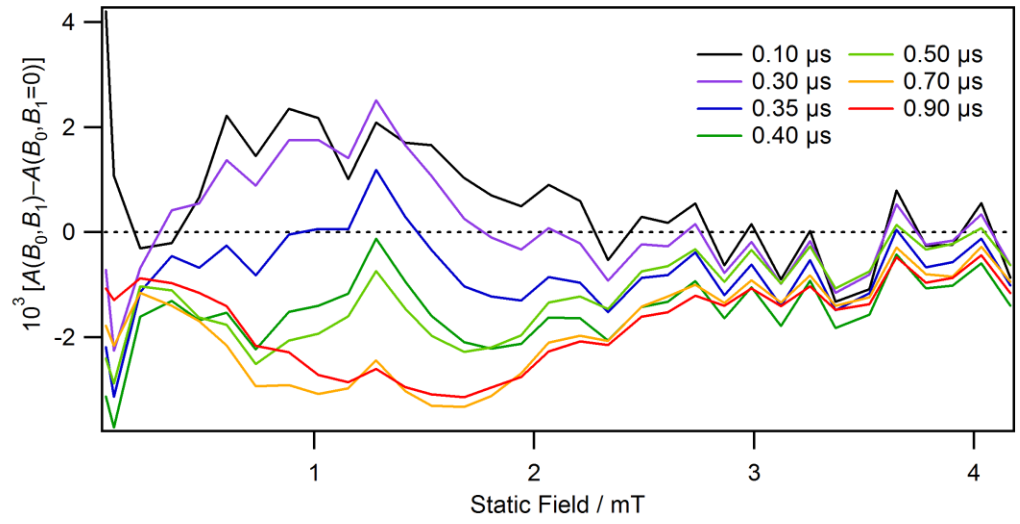

Figure S6. Time-resolved RYDMR spectra as a function of time. The centre of a 100 ns wide averaging window is as indicated. Spectra were recorded with static and 36 MHz oscillating fields parallel, $B_1 = 0.17$ mT.

5. Invariance of simulations to hyperfine couplings

Figure S7 presents simulated data for 4 different hyperfine coupling conditions. The two lines marked "Equal HFCCs" and "Unequal HFCCs" provide a check that use of identical hyperfine couplings does not produce anomalous simulation results due to degeneracy in the radical pair energy levels. "Equal HFCCs" has both hyperfine couplings set to the same value of 0.6 mT. "Unequal HFCCs" has the couplings perturbed such that the values of the couplings differ by 0.06 mT (10% of the original value), while the root-mean-square value of the hyperfine couplings remains the same. This gives HFCCs of 0.62925 mT and 0.56925 mT. These traces are virtually indistinguishable showing that, in this instance, having degenerate hyperfine couplings does not introduce anomalies.

The hyperfine couplings of the "Unequal HFCCs" case were perturbed by increasing or decreasing both values by 10%, to generate the values for the two other traces – "Larger HFCCs" and "Smaller HFCCs". In the "Larger HFCCs" case this gives hyperfine coupling constants of 0.69217 mT and 0.62617 mT, and in the "Smaller HFCCs" case the constants are 0.56632 mT and 0.51232 mT. Although these changes cause minor variations in the overall shape of the curve they verify that it is relatively insensitive to the precise hyperfine coupling constants used, and changes in the zero-crossing time of the data are significantly smaller than 10%. This insensitivity to the exact hyperfine coupling constants chosen for the simulation justifies our decision to use physically plausible values to recreate the width of the carotenoid hyperfine spectrum but not to attempt to match precisely any (or all) of the 22 significant (> 100 μT) couplings in the real radical [K. Maeda et al., *Nature*, **453**, 387–390, (2008)].

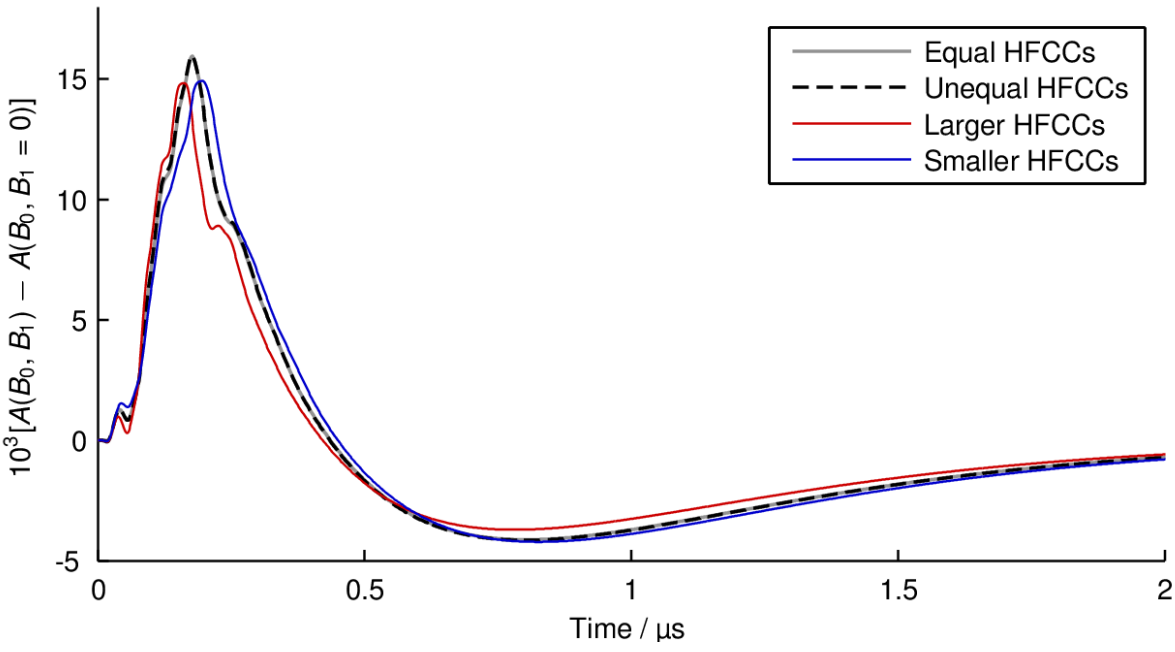

Figure S7. Simulated RYDMR time-profiles. Two hyperfine couplings are present on the same radical which are: (i) equal at 0.6 mT; (ii) unequal at 0.62925 and 0.56925 mT, which gives a 0.06mT (10%) difference in the values whilst maintaining the root-mean-square (RMS) total coupling as in (i); (iii) hyperfine couplings of 0.69217 and 0.62617mT corresponding to a 10% increase in RMS with respect to (ii), and (iv) hyperfine couplings of 0.56632 and 0.51232 mT corresponding to a 10% decrease in RMS total coupling with respect to (ii). All other parameters are as indicated in Figure 5B.